Published online 13 October 2017 *Nucleic Acids Research, 2017, Vol. 45, No. 21* **12441–12454**
doi: 10.1093/nar/gkx931

NF90–NF45 is a selective RNA chaperone that rearranges viral and cellular riboswitches: biochemical analysis of a virus host factor activity

Tobias Schmidt*, Susann Friedrich, Ralph Peter Golbik and Sven-Erik Behrens*

Institute of Biochemistry and Biotechnology (NFI), Section Microbial Biotechnology, Martin Luther University Halle-Wittenberg, Kurt-Mothes-Str. 3, D-06120 Halle/Saale, Germany

Received August 08, 2017; Revised September 22, 2017; Editorial Decision September 26, 2017; Accepted October 10, 2017

ABSTRACT

The heterodimer NF90–NF45 is an RNA-binding protein complex that modulates the expression of various cellular mRNAs on the post-transcriptional level. Furthermore, it acts as a host factor that supports the replication of several RNA viruses. The molecular mechanisms underlying these activities have yet to be elucidated. Recently, we showed that the RNA-binding capabilities and binding specificity of NF90 considerably improves when it forms a complex with NF45. Here, we demonstrate that NF90 has a substrate-selective RNA chaperone activity (RCA) involving RNA annealing and strand displacement activities. The mechanism of the NF90-catalyzed RNA annealing was elucidated to comprise a combination of 'matchmaking' and compensation of repulsive charges, which finally results in the population of dsRNA products. Heterodimer formation with NF45 enhances 'matchmaking' of complementary ssRNAs and substantially increases the efficiency of NF90's RCA. During investigations of the relevance of the NF90–NF45 RCA, the complex was shown to stimulate the first step in the RNA replication process of hepatitis C virus (HCV) *in vitro* and to stabilize a regulatory element within the mRNA of vascular endothelial growth factor (VEGF) by protein-guided changes of the RNAs' structures. Thus, our study reveals how the intrinsic properties of an RNA-binding protein determine its biological activities.

INTRODUCTION

NF90 is a double-stranded (ds) RNA-binding protein that is crucially involved in RNA metabolism. NF90's role as a post-transcriptional regulator of gene expression is best understood where it binds to structured 3′-untranslated regions (3′UTRs) of various mRNAs and modulates the RNA's turnover and availability for translation (1–3). For example, under hypoxic stress, NF90 stabilizes the mRNA of vascular endothelial growth factor (VEGF) by associating with a defined structural element in the mRNA's 3′-UTR (Supplementary Figure S1A) (4). NF90 also interacts with the mRNA-mimicking genomes of positive-strand RNA viruses. Thus, several members of the *Flaviviridae* family, e.g. hepatitis C virus (HCV), dengue virus (DV) and bovine viral diarrhea virus (BVDV), were found to exploit NF90 as a host factor that supports viral amplification (5–9). With HCV and BVDV, NF90 was shown to bind to defined RNA motifs close to the 3′-end of the viral RNA (6–8) (Supplementary Figure S1B) and to stimulate the viral RNA replication process (6–9). The molecular mechanisms underlying this pathogen-supporting activity of NF90 were hitherto unknown.

NF90 is 706 amino acids (aa) long and contains an N-terminal domain associated with zinc-fingers (DZF). Moreover, the protein contains a tandem pair of dsRNA-binding motifs (dsRBMs) and an RGG/RG motif in its otherwise structurally disordered C-terminus (aa 381–706). DsRBMs are known to associate with high affinity to dsRNA (10) while RGG/RG motifs preferentially interact with single-stranded (ss) RNA (11,12). Our own studies and those of others have shown that a dynamic and cooperative interplay of all three RBMs contributes to NF90's overall RNA binding properties (13–15) and enables the protein to distinguish between different features of target RNAs (15).

NF90 is indicated to interact with several other protein partners (16); however, in most investigated cell types, it exists predominantly as a complex together with the 390 aa NF45 protein. The core of the NF90–NF45 complex is formed by the interaction between the N-terminal DZF of NF90 and the DZF of NF45, but the C-terminus of NF90 is also suggested to contribute to heterodimer formation (14,17–19). Recently, we reported that complex formation between NF90 and NF45 results in a mutual thermody-

*To whom correspondence should be addressed. Tel: +49 3455 5249 60; Fax: +49 3455 5273 87; Email: sven.behrens@biochemtech.uni-halle.de
Correspondence may also be addressed to Tobias Schmidt. Email: ts300@le.ac.uk
Present address: Tobias Schmidt, Medical Research Council Toxicology Unit, Hodgkin Building, Lancaster Road, Leicester LE1 9HN, UK.

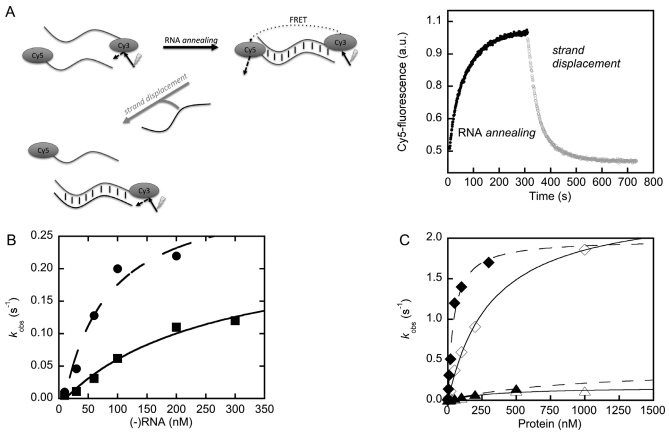

Figure 1. NF90$_b$ is an RNA '*annealer*'. (**A**) Schematic representation of the elementary reactions of an RNA chaperone activity and the experimental setup in this study. Complementary ssRNAs were labeled at the 5′-end with Cy3 and Cy5, respectively. Upon RNA annealing (black arrow) the FRET between Cy3 and Cy5 is monitored to follow RNA–RNA interaction (black trace in the plot). For an induction of strand displacement, an excessive amount of a non-labeled competitor RNA was added, which eventually leads to a strand exchange (grey arrow) and a decrease in FRET (gray trace in plot). (**B**) The RNA annealing reactions of 10 nM RaSc-Cy5 strand (square) and HCV-SL3 Cy5-strand (circle) RNAs were monitored at increasing concentrations of the complementary Cy3-RNA strands**.** Progress curves were investigated according to a second-order reaction (Equation 1), which yielded apparent rate constants k_{obs}. k_{obs} was plotted versus the concentration of the Cy3-RNA strand and fitted according to Equation 2. Kinetic parameters are summarized in Table 2. (**C**) The RNA annealing reactions (10 nM each strand) of RaSc (full symbols) and dsHCV-SL3 ssRNAs (open symbols) in the presence of NF90$_b$wt (triangle) and NF90$_b$wt–NF45 (diamond) were investigated as for (B). Kinetic parameters are summarized in Table 2. A minimum of two kinetic traces were averaged and investigated by Equation (1), the errors of the fitting routine were in the range of 15%.

namic stabilization of the proteins, which leads to changes in the RNA-binding mode and significantly enhances the RNA-binding affinity of NF90 (19).

Several cellular proteins have been described to trigger the folding of functionally active conformations of RNA molecules and to regulate, *via* this function, diverse paths in cellular RNA metabolism (20). According to the current definition, proteins are referred to have an 'RNA chaperone activity', RCA, if they are capable of resolving mis-folded RNA structures *in vitro* and if they share activities in promoting RNA–RNA interactions by 'RNA annealing' or in separating RNA duplexes by 'strand displacement' (Figure 1A) (20,21). In the life cycle of RNA viruses, an essential step involves the folding of the viral RNAs into biologically relevant conformations (22). Thus, in several cases, cellular and viral RNA chaperones were suggested to assist viral infection processes by facilitating conformational transitions of RNA molecules (23–28). The exact mechanisms of how these proteins exert these activities have yet to be investigated.

Here, we report a hitherto unknown RCA of NF90, which manifests itself predominantly as an RNA annealing activity. Heterodimer formation between NF90 and NF45 strongly improves the efficiency of the RCA, and the underlying mechanism was characterized as a combination of 'matchmaking' and compensation of repulsive charges. Furthermore, we demonstrate that NF90–NF45, but neither a RCA-deficient complex variant nor NF90 alone, stimulates the first step of the HCV RNA replication process *in vitro* and that NF90–NF45 is able to elicit alterations in the structure of the viral RNA. Along the same line, we observed that NF90–NF45 increases the stability of a regulatory double-stranded region within the VEGF mRNA's 3′UTR. Together, the findings of this study suggest that the RCA-driven changes in RNA structures represents a further essential functional determinant of the already diverse activities attributed to NF90 and NF90–NF45.

MATERIALS AND METHODS

Preparation of recombinant NF90, NF45 and reconstitution of NF90–NF45 and variants

NF90, and variants of NF90 and NF45 were generated and purified as reported earlier (15,19). The proteins were produced in *Escherichia coli* BL21 (DE3) RP and isolated from inclusion bodies. Purification was performed under denaturing conditions applying a cation-exchange-chromatography column. Refolding of the individual proteins was achieved using a rapid-dilution/pulse-refolding approach in assay buffer [50 mM Na-phosphate, pH 7.2, 100 mM NaCl, 5% (v/v) glycerol, 1 mM TCEP] supplemented with arginine. Refolded protein solutions were finally applied to affinity and size-exclusion chromatography columns; each column was pre-equilibrated in assay buffer. Heterodimeric NF90–NF45 was produced by co-refolding equimolar amounts of NF90 and NF45 following the same procedure as with the individual proteins. The homogeneity of the prepared proteins and the heterodimeric complex was confirmed as described (15,19).

Oligonucleotides

The 5′-fluorophor-labeled oligonucleotides used in this study (see Table 1) were purchased from IBA GmbH (Goettingen, Germany). Concentrations were calculated by determining the absorbance at 260 nm using extinction coefficients provided by the supplier. The dsRNAs were prepared by mixing of the corresponding ssRNAs in equimolar ratio, heating to 95°C followed by slow cooling and final purification by non-denaturing PAGE before storage at –80°C.

RNA annealing/strand displacement assay

10 nM of Cy3-labeled HCV-SL3 or RaSc (Table 1) were incubated with the indicated concentrations of protein in assay buffer for 5 min at 20°C. RNA annealing was induced by the addition of the complementary Cy5-labeled RNA strand (10 nM final) and readings were taken for 220 s. The reaction was monitored on a FluoroMax-4 (Jobin Yvon, France) by following a FRET signal, which occurred exclusively when we applied complementary RNA strands (see Supplementary Figure S2A and S2C). Excitation was done at 535 nm (Cy3) and emission was read at 680 nm (Cy5). Fluorescence intensities relative to intensities at $t =$ 220 s were plotted versus time, and progress curves fitted according to a second-order reaction (Equation 1, (21)) using

Table 1. Synthetic fluorophor-labeled RNA molecules that were applied for binding studies

Substrate	Sequence[a]
dsHCV-SL3	Cy5–5′-UGUUGGCUCCAUCUU-3′ 3′-ACAACCGAGGUAGAA-5′-Cy3
HCV-SL3-bulge	Cy5–5′-UGUUGGCUCCAUCUU-3′ 3′ACAACCACAAUAGAA-5′-Cy3
HCV-SL3-fork	Cy5–5′-UGUUGGCUCCAUCUU-3′ 3′-ACAACCGAGGUCAUU-5′-Cy3
RaSc	Cy5–5′-AAGUGUAAAAUCUCUAGUAGU-3′ 3′-UUCACAUUUUAGAGAUCAUCA-5′-Cy3
RaSc-bulge	Cy5–5′-AAGUGUAAAAUCUCUAGUAGU-3′ 3′-UUCACAUCCCCACGAUCAUCA-5′Cy3
RaSc-fork	Cy5–5′-AAGUGUAAAAUCUCUAGUAGU-3′ 3′-UUCACAUUUUAGAGACACCAC-5′Cy3
VEGF HSR-SL	5′FAM-AUAUAUAUAUUAUAUAUAUAUAAAAAUAAAUAUCUC UAUUUUAUAUAUAUAAAAUAUAUAUAU-3′

[a]Underlined nucleotides do not form base pairs in the dsRNA.

KaleidaGraph™ (Synergy Software) yielding the observed rate constants k_{obs}.

$$\frac{F}{F_{220}} = C + \gamma \cdot \left(1 - \frac{1}{k_{obs} \cdot t + 1}\right) \quad (1)$$

F and F_{220} are the fluorescence intensity at t and 220 s. γ is the signal amplitude. c is the offset. k_{obs} is the observed reaction rate constant.

The dependence of k_{obs} on the protein concentration was further investigated according to a hyperbola-model, where k_{obs} equals k_{cat} when $[S]_0 >> K_M$ (Equation 2, (29))

$$k_{obs} = \frac{k_{cat} \cdot [S]_0}{K_M + [S]_0} \quad (2)$$

k_{obs} is the observed reaction rate constant at a protein or RNA concentration $[S]_0$. K_M is the protein concentration, where k_{obs} is half-maximal and k_{cat} is the catalytic rate constant at $[S]_0 >> K_M$.

Catalytic efficiencies were calculated from k_{cat}/K_M.

Second-order rate constants k_{on} were determined from the initial linear phase of the plot of k_{obs} versus $[S]_0$ according to Equation (3).

$$k_{obs} = k_{on} \cdot [S]_0 + k_{off} \quad (3)$$

k_{obs}, k_{on} and k_{off} represent the observed, the second-order rate constant and the off-rate, respectively. $[S]_0$ is the protein or Cy5–ssRNA concentration.

Strand displacement reactions were performed according to Rajkowitsch and Schroeder (21). Briefly, RNA annealing reactions were allowed to proceed for 300 s prior to the addition of a 10-fold excess of unlabeled RNA strand together with indicated amounts of protein. The reaction was allowed to continue for another 300 s. k_{obs}- and k_{on}-values were obtained as described above for the RNA annealing reactions.

For all kinetic reactions, at least a duplicate of traces were averaged and applied to software-assisted calculations. The errors of resulting kinetic parameters that were obtained in the course of the fitting-routine were in the range of 15%.

Arrhenius analysis

RNA annealing reactions were performed as described above but at different temperatures. Apparent reaction rate constants k_{obs} were determined from progress curves using Equation (1). Rate constants were normalized to the protein concentration to compensate for different specific activities of the proteins. Resulting second-order rate constants were further investigated by an Arrhenius analysis using the following Equations (4)-(7).

$$\ln\ k_{obs} = -\frac{E_A}{RT} + C \quad (4)$$

$$\Delta G^{\neq} = -RT \cdot \ln\left(\frac{k \cdot h}{k_B \cdot T}\right) \quad (5)$$

$$\Delta H^{\neq} = E_A - RT \quad (6)$$

$$\Delta S^{\neq} = -\frac{1}{T} \cdot (\Delta G^{\neq} - \Delta H^{\neq}) \quad (7)$$

k_{obs} and k are the observed and second-order rate constant, E_A is the Arrhenius activation energy. R is the gas constant. T is the absolute temperature. C is constant. h is Planck's constant. k_B is Boltzmann's constant. $\Delta G^{\neq}$, $\Delta H^{\neq}$ and $\Delta S^{\neq}$ are the changes in free activation energy, in-activation enthalpy and in-activation entropy, respectively.

Generation of viral RNA templates

RNAs were transcribed with T7 RNA-polymerase from PCR products (standard procedures) that were generated with specific primers (Supplementary Table S1) from a pUC19-Con1 plasmid that contained the cDNA coding for a bicistronic replicon of HCV-1b (Con1 isolate) (30).

Polymerase assay

The assay was carried out in polymerase assay buffer [PAB; 20 mM HEPES/NaOH, pH 7.1, 50 mM NaCl, 20% (v/v) glycerol, 6.5 mM $MgCl_2$, 0.5 mM $MnCl_2$, 1 mM DTT, 0.5 mM r(ATP,UTP,GTP)] supplemented with 20 μCi [α-^{32}P-]CTP, 30 nM template RNA and 100 nM NS5B (HCV-1b

Con1) at 20 or 37°C in a final volume of 40 μl. The viral 3′-UTR plus the 5BSL3 region (5BSL3_3UTR), the X-tail only and poly-rC (1 μg) served as template RNA (Figure 4A). For reactions with poly-rC, [α-^{32}P-]GTP was used instead of [α-^{32}P-]CTP. When protein was investigated for an effect on the reaction, protein and template RNA were pre-incubated and allowed to equilibrate for 10 min at 20°C in PAB, before the reaction was started by the addition of NS5B. After 1 h, the reactions were stopped by phenol-chloroform extraction and radioactivity was measured applying scintillation counting.

Thermal denaturation of RNA

30 nM of the viral RNA templates were incubated with the indicated concentrations of protein in PAB without $MnCl_2$. Thermal denaturation was monitored in the range from 30 to 90°C at 0.4 K min^{-1} by recording the absorbance change at a constant wavelength of 268 nm on a Jasco-V550 equipped with temperature control unit ETC-505T. At this wavelength, maximal changes in the absorbance during unfolding were observed (not shown). Absorbance changes relative to the signal at 30°C were plotted against the temperature and transition curves were analyzed semi-quantitatively by calculating the melting points (T_M) from the first derivative of each curve.

For VEGF HSR-SL RNA (IBA Goettingen, Table 1), 500 nM of RNA were incubated with the indicated concentrations of protein in assay buffer. Thermal denaturation was conducted as described above but in the temperature range from 10 to 90°C at 0.4 K min^{-1}. Absorbance changes were normalized and analyzed according to Riechmann *et al.* (31) using Equations (8) and (9) for analysis of the melting of VEGF RNA (unfolding of stem–loop).

$$A = \frac{(A_N + m_N T) - [A_N + m_N T - (A_U + m_U T)] \cdot e^{\frac{-\Delta G^0}{RT}}}{1 + e^{\frac{-\Delta G^0}{RT}}} \quad (8)$$

$$\Delta G^0 = \Delta H \cdot \left(1 - \frac{T}{T_M}\right) + \Delta C_p \left(T - T_M - T \cdot \ln \frac{T}{T_M}\right) \quad (9)$$

A is the signal amplitude at temperature T, A_N and A_U are the signal amplitudes of the native and unfolded state extrapolated to $T = 0$ K, respectively. m_N and m_U are the slopes of the baselines of the native and unfolded state; T_M is the transition midpoint, R is the gas constant, ΔC_p is the difference in heat capacity between the native and unfolded state, and $\Delta G°$ and $\Delta H°$ are the changes in free energy and enthalpy in equilibrium, respectively.

RESULTS

NF90$_b$ and the heterodimer NF90$_b$–NF45 display an RNA annealing activity

NF90 and/or NF90–NF45 were earlier reported to be subunits of various nucleic acid-rearranging protein complexes (6,7,32,33). This led to the hypothesis that NF90, besides acting as a classical RNA-binding protein, might also function as an RNA chaperone. To test this, we took advantage of the assay developed by Rajkowitsch and Schroeder (21) using short, complementary Cy3/Cy5-fluorophor labeled ssRNAs that enable the monitoring of RNA annealing and strand displacement processes by time-dependent fluorescence resonance-energy transfer (FRET; Figure 1A). On the one hand, we applied the same RNA molecules as these authors (referred here to as 'RaSc'). On the other hand, we tested RNAs, which corresponded to a fully double-stranded version of the SL3 stem–loop motif that was identified by us to be part of the NF90–NF45 binding region in the HCV RNA (6), referred to here as 'dsHCV-SL3'; Table 1 and Supplementary Figure S1B). Control 'RNA-only' reactions validated the assay. By mixing the complementary ssRNAs, a signal change was measured, and the apparent rate constants (k_{obs}) of RNA-RNA interactions were determined. When we performed this assay with the RaSc RNAs, our measurements correlated well with the data reported by Rajkowitsch and Schroeder (Figure 1B and Supplementary Figure S2).

Interestingly, in succeeding experiments, which were carried out with the Cy-labeled RNAs and in the presence of homogenous preparations of NF90 (isoform NF90$_b$) or the NF90$_b$–NF45 heterodimer, the RNA annealing reactions were found to be significantly accelerated (Figure 1C). This was not observed in control reactions, which applied either the individual NF45, an unrelated RNA-binding protein, hnRNP H1 (28), or NF90$_b$ or NF90$_b$–NF45 and non-complementary RNAs (Supplementary Figure S2). The apparent rate constant k_{obs} approximated a hyperbolic 'saturation' behavior, which, in the case of the RNA-only reactions was limited by the concentrations of the RNAs (Figure 1B). In the presence of NF90$_b$ or NF90$_b$–NF45, it depended on the protein concentration (Figure 1C). Since the reaction applied two ssRNAs, we explained this by the formation of a reaction intermediate involving both RNA strands (29,34,35). Accordingly, the linear part of the plot of k_{obs} versus the RNA or protein concentration (Figure 1B-C) could be investigated to yield the second-order rate constant k_{on} as a measure of the initial association step of the two RNA strands. At higher concentrations, the decay of the intermediate became rate limiting as k_{cat}; catalytic efficiencies were calculated from k_{cat}/K_M (further explained in Materials and Methods).

The analyses revealed that with both the RaSc and the dsHCV-SL3 RNAs, the heterodimer NF90$_b$–NF45 showed a 10-fold increase in k_{cat} and a 50-fold increase in k_{on} as compared to the NF90$_b$ monomer (Table 2). Thus, the efficiency (k_{cat}/K_M) of the RNA annealing activity (RAA) of NF90$_b$–NF45 versus the monomeric NF90$_b$ was enhanced by 13-fold with dsHCV-SL3, and 70-fold with RaSc (Table 2). The interesting fact that NF90–NF45 displayed different RAAs with the two types of RNA substrates was even more apparent when we correlated the 'protein-catalyzed' with the 'RNA-only' reactions. Thus, NF90$_b$–NF45 improved the RNA annealing efficiency of RaSc by 62-fold, while it was 2.5-fold with dsHCV-SL3 (Table 2). In contrast, the NF90$_b$ monomer apparently did not improve RNA annealing efficiency of RaSc and impaired the RNA annealing of dsHCV-SL3 by 5-fold in comparison to the 'RNA only' reaction. With the applied RNA substrates, and under the chosen experimental conditions, neither NF90$_b$ nor NF90$_b$–NF45 showed a strand-displacement activity.

Table 2. Kinetic parameters of the RNA annealing of $NF90_b$wt and $NF90_b$wt–NF45 variants

		k_{on} (10^6 M^{-1} s^{-1})	k_{cat} (s^{-1})	k_{cat}/K_M (10^6 M^{-1} s^{-1})
RNA	dsHCV-SL3	2	0.4	3
	RaSc	0.4	0.2	0.8
$NF90_b$wt	dsHCV-SL3	0.1	0.2	0.6
	RaSc	0.3	0.2	0.7
$NF90_b$wt–NF45	dsHCV-SL3	5	2.5	8
	RaSc	15	2.1	50
$NF90_b^{S651E}$–NF45		1	1.2	1
$NF90_b^{F432,559A}$–NF45		3	3.8	6
$NF90_b\Delta C63$	dsHCV-SL3		no RCA detected	
$NF90_b\Delta C63$–NF45		0.2	0.2	0.5
$NF90_b\Delta C46$		0.03	0.12	0.05
$NF90_b\Delta C46$–NF45		0.5	>0.5	~0.5

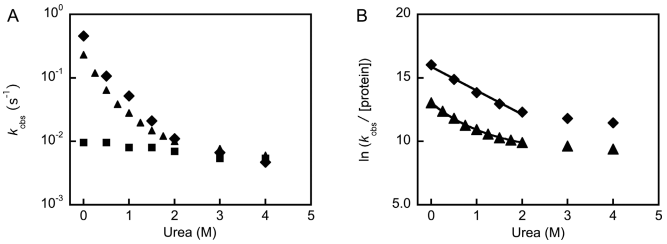

Figure 2. Structural elements of NF90 and NF45 that are stabilized during heterodimerization contribute to the RNA annealing activity of the NF90–NF45. (**A**) The RNA annealing reactions of dsHCV-SL3 in the absence (square) and presence (triangle) of $NF90_b$wt or $NF90_b$wt–NF45 (diamond) were investigated at increasing concentrations of urea. Progress curves were investigated according to a second-order reaction (Equation 1), which yielded apparent rate constants k_{obs}. k_{obs} was plotted versus the concentration of urea. (**B**) Same as (A), but k_{obs} was normalized to the applied protein concentration. The data were fit according to a linear or exponential regression. At least two kinetic traces were averaged and investigated by Equation (1); the errors of the fitting routine were in the range of 10%. Best-fit models were statistically challenged using an F-test and a false-rejection of $P < 0.01$.

Structural elements of $NF90_b$ and NF45 that are stabilized during heterodimer formation contribute to the RNA annealing function of NF90–NF45.

Previous chemical unfolding studies of $NF90_b$ and $NF90_b$–NF45 had demonstrated that the formation of the complex results in a thermodynamic stabilization of structural elements of the $NF90_b$ and NF45 components (19). To test whether the improved RCA of $NF90_b$–NF45 correlated with this increased stability of the heterodimer, we assayed the RAA of $NF90_b$–NF45 with dsHCV-SL3 in the presence of 0 to 4 M urea. Within this concentration range of the denaturant, the stabilization effect of heterodimer formation was earlier shown to be significant, and the individual as well as the NF45-complexed $NF90_b$ were known to bind RNA under these conditions (19). Control 'RNA-only' experiments revealed a negligible influence of the denaturant on the RNA-RNA interactions (Figure 2A). However, the acceleration of the RNA-annealing reaction by $NF90_b$ and $NF90_b$–NF45 was only detectable up to 2–3 M of denaturant; at higher concentrations, the k_{obs} values approximated the numbers that were measured with the 'RNA-only' reactions (Figure 2A). To compare directly the different RAA of $NF90_b$ and $NF90_b$–NF45, k_{obs} was related to the protein concentration and plotted as ln (k_{obs}/[protein]) against the respective concentrations of urea (Figure 2B). This describes a linear free energy method (LEM) (15,19), which is established to investigate correlations between structure and function of different enzymes (19,36,37). Thus, a linear correlation of the LEM indicates the integrity of structural elements of the protein that are involved in the enzymatic reaction. We investigated the data obtained with $NF90_b$ and $NF90_b$–NF45 applying an F-test that compared a line versus an exponential model with a false-rejection of $P < 0.01$. As shown in Figure 2B, this revealed a linear correlation for the RAA of the $NF90_b$–NF45 heterodimer in the range of 0–2 M urea, while this was not the case for $NF90_b$. Hence, we considered these results as an indication that functional elements of NF90 and/or NF45, which contribute to the RAA, are stabilized within the heterodimer.

The RNA-binding motifs of $NF90_b$ contribute differently to the RNA annealing activity

The above findings directed us to evaluate next the contributions of the individual RNA-binding motifs (RBMs) of $NF90_b$ in the RNA annealing reaction. For this, we examined two complex variants, $NF90_b^{S651E}$–NF45 and $NF90_b^{F432,559A}$–NF45 that had been characterized earlier, and in which amino acid substitutions in $NF90_b$ impaired the RGG motif or both dsRBMs, respectively (19). The RGG motif was modified by pseudophosphorylation of S651 (exchange to glutamic acid) while the dsRBMs were inactivated by the exchange of functionally important phenylalanines to alanines (10,19,38–40).

Performing analogous experiments as in Figure 1 with the dsHCV SL-3 RNA, we determined a second-order rate constant k_{on} with $NF90_b^{F432,559A}$–NF45, which was only slightly reduced in comparison to that of $NF90_b$wt–NF45, (Figure 3A and Table 2). While k_{cat} was slightly increased (Table 2), the efficiency of the RNA-annealing reaction of $NF90_b^{F432,559A}$–NF45 was nevertheless comparable to that of the wild-type complex (Table 2). Conversely, the pseudophosphorylated complex $NF90_b^{S651E}$–NF45 showed an evident decrease in k_{on} and k_{cat} by 5- and 2-fold, respectively, *i.e.*, the efficiency of the RAA of this variant was about a factor of 8 lower than that of the wild-type complex (Table 2). As these data indicated an important role of the C-terminal region of NF90 in the RAA, we further investigated the RCA of other, previously characterized NF90 variants, namely $NF90_b\Delta C63$ and $NF90_b\Delta C46$

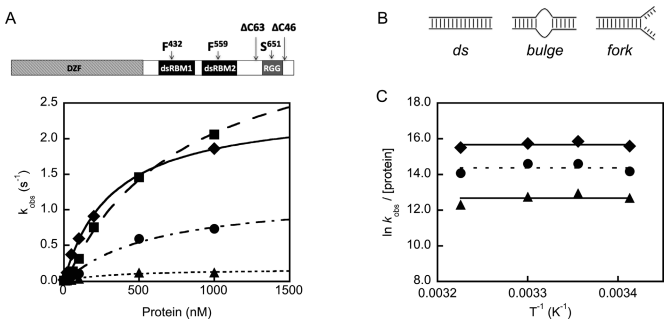

Figure 3. The role of the RNA-binding motifs of NF90 for its RNA annealing activity. (**A**) The upper panel represents schematically the domain organization of NF90; DZF—dimerization zinc-finger, dsRBM – double-stranded RNA-binding motif, RGG—arginine–glycine-rich motif. Arrows indicate the position of introduced amino acids substitution. The plot displays the RNA-annealing reactions of dsHCV-SL3 monitored at increasing concentrations of $NF90_b$wt (triangle), $NF90_b$wt–NF45 (diamond), $NF90_b^{S651E}$–NF45 (circle) and $NF90_b^{F432,559A}$–NF45 (square). Progress curves were investigated according to a second-order reaction (Equation 1), which yielded apparent rate constants k_{obs}. k_{obs} was plotted versus the protein concentration and fitted according to Equation (2). Kinetic parameters are summarized in Table 2. (**B**) Schematic representation of the structural organization of the applied RNA substrates that were designed to contain non-complementary internal (bulge) or ending regions (fork). (**C**) The RNA annealing reactions of dsHCV-SL3 were monitored in the presence of $NF90_b$wt (triangle), $NF90_b$wt–NF45 (diamond) and $NF90_b^{S651E}$–NF45 (circle) at increasing temperatures**.** Progress curves were investigated according to a second-order reaction (Equation 1), which yielded apparent rate constants k_{obs} and these were normalized to the applied protein concentration and plotted versus 1/T. The data were further investigated according to Equations (4)–(7) to reveal the thermodynamic properties of the transition state of the reaction. Parameters are summarized in Table 4. At least two kinetic traces were averaged and investigated by Equation (1), and the errors of the fitting routine were in the range of 10%

(15). These contain major C-terminal truncations, which included (ΔC63) or did not include (ΔC46) the RGG motif (Figure 3A). Annealing experiments demonstrated that $NF90_b$ΔC63 did not accelerate the RNA annealing, while $NF90_b$ΔC46 showed a very weak catalysis (Table 2). Subsequent tests with the respective $NF90_b$ΔC63–NF45 and $NF90_b$ΔC46–NF45 heterodimers revealed that the presence of NF45, while increasing the efficiency of the variant's RAA, it did not restore the low efficiency of the NF90 variant's RCA to wild-type levels (Table 2). Hence, these findings supported and extended earlier observations demonstrating that the individual contributions of NF45 to RNA binding and RNA annealing is rather low (19) and that it requires full-length NF90 for most efficient RNA annealing. Furthermore, the data underpinned that NF90's RNA-binding motifs contribute differently to the RCA.

NF90 is a substrate-selective RNA chaperone

Several of NF90's native dsRNA targets are not fully double-stranded but contain internal or terminal mismatches. Accordingly, the next experiment investigated the RAA of $NF90_b$/$NF90_b$–NF45 with RNA substrates that show considerably different structural properties. To generate a fork-like (referred to as HCV-SL3-fork) or bulged structure (referred to as HCV-SL3-bulge; see Figure 3B), we introduced 4 nt-substitutions at the termini and in the center of the dsHCV-SL3 RNA, respectively. Initially, we characterized the thermodynamic properties of these RNAs by performing thermal denaturation studies to determine the melting enthalpy (ΔH_{TM}). As would be anticipated from the lower proportion of base pairings, both the fork and bulge RNAs showed significantly lower ΔH_{TM} values than the dsHCV-SL3. Still, both modified dsRNAs showed thermodynamic stabilities, which were sufficient to perform annealing measurements under the applied assay conditions (see Supplementary Results and Table S2).

In 'non-catalyzed' RNA-only annealing reactions that applied the fork- or bulge substrates, the dependency of k_{obs} on the RNA concentration turned out not to have a hyperbolic profile (data not shown). For that reason, we investigated only k_{on}. This revealed that the non-catalyzed RNA-annealing reactions of HCV-SL3-bulge and HCV-SL3-fork proceeded with second-order rate constants that were ca. 30-fold reduced in comparison to the fully complementary dsHCV-SL3 (Table 3).

With HCV-SL3-fork, both $NF90_b$wt and $NF90_b$wt–NF45 accelerated the RNA-RNA interaction in a concentration-dependent manner but the corresponding k_{on}-values were about 10- and 5-fold reduced with respect to the reactions that applied dsHCV-SL3 (Table 3). However, analogous to what we observed earlier with dsHCV-SL3, the heterodimer showed an increase in k_{on} by about 100-fold as compared to the individual NF90. Interestingly, none of the proteins accelerated the RNA annealing of the HCV-SL3-bulge RNAs (for each reaction $k_{obs} = 0.01\ s^{-1}$).

As these findings suggested a selectivity of $NF90_b$ in the RNA annealing reaction, we were prompted to examine a strand displacement (SD) activity with the modified RNA substrates. Considering that neither $NF90_b$wt nor $NF90_b$wt–NF45 performed a strand displacement on fully complementary substrates, we performed the assay in such a way that the mismatched strand was displaced by a fully complementary strand (see Figure 1A). Thus, in the absence of protein, HCV-SL3-fork was not susceptible to a strand displacement, while HCV-SL3-bulge readily underwent displacement with a first-order rate constant of $k_{obs} = 0.02\ s^{-1}$.

Strikingly, in the presence of $NF90_b$wt or $NF90_b$wt–NF45, we observed catalysis of the strand displacement reaction in a concentration-dependent manner on both RNA substrates (Table 3 and Supplementary Figure S3). With HCV-SL3-bulge, the k_{on}-values that were measured with $NF90_b$wt and $NF90_b$wt–NF45 were very similar to those of the corresponding annealing reactions with dsHCV-SL3 (Table 3). In contrast, the rate constants and k_{on} values that were measured for strand displacement with HCV-SL3-fork were much lower than those measured for the annealing of dsHCV-SL3: e.g. with $NF90_b$–NF45 it was 250-fold lower (Table 3). As in the annealing reaction, the heterodimer showed strand displacement activities that were 10-fold (HCV-SL3-fork) or 35-fold (HCV-SL3-bulge) increased in comparison to those of the NF90 monomer. In conclusion, these experiments revealed the importance of structural features of the RNA substrates for the protein-catalyzed RNA annealing. Moreover, $NF90_b$ and $NF90_b$–NF45 were demonstrated to anneal, but also to displace, RNA strands and, therefore, to meet both the criteria of RNA chaperones (see Introduction).

Table 3. Kinetic parameters of the RNA annealing and strand displacement of $NF90_b$wt and $NF90_b$wt–NF45 on related but structurally different RNAs

		RNA annealing k_{on} (10^6 M^{-1} s^{-1})	strand displacement k_{on} (10^6 M^{-1} s^{-1})
dsHCV-SL3	RNA only	2	no SD
	$NF90_b$wt	0.1	no SD
	$NF90_b$wt–NF45	5	no SD
HCV-SL3-fork	RNA only	0.07	no SD
	$NF90_b$wt	0.01	0.002
	$NF90_b$wt–NF45	0.93	0.02
HCV-SL3-bulge	RNA only	0.06	0.02*
	$NF90_b$wt	no annealing	0.2
	$NF90_b$wt–NF45	no annealing	7

*Observed rate constant for assay conditions 10 nM dsRNA and 100 nM unlabeled strand.

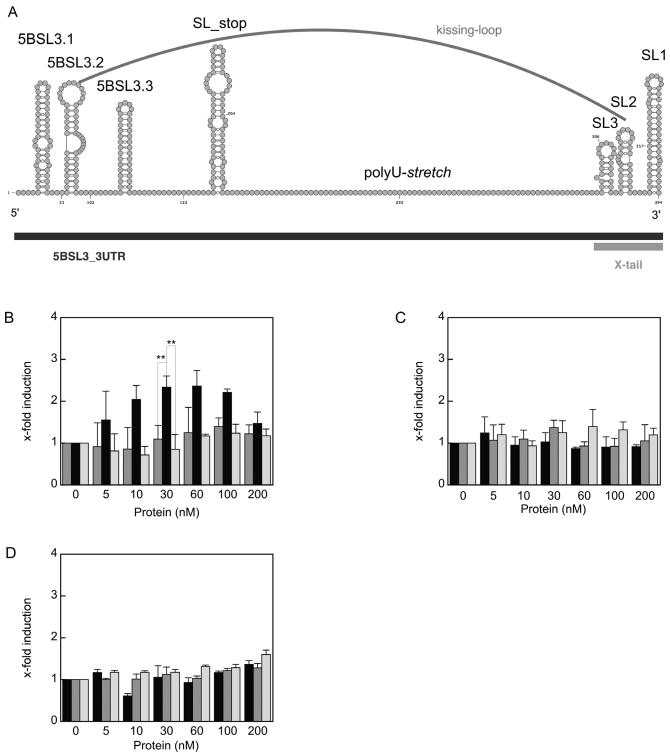

Figure 4. $NF90_b$wt–NF45 stimulates viral RNA synthesis *in vitro*. (**A**) Schematic representation of the secondary and tertiary structures formed by the 3′-end of the HCV RNA genome. Note that the structures shown were experimentally confirmed (47). In this study, the RNAs 5BSL3_3UTR (black bar), which contains each of the indicated structural elements, and X-tail (grey bar), which contains SL1, SL2 and SL3 only, were applied as templates to the performed RdRp assays. (**B**–**D**) RdRp assays using 30 nM 5BSL3_3UTR (**B**), 30 nM X-tail (**C**) or 1 μg poly(rC) (**D**) as templates were complemented with the indicated amounts of $NF90_b$wt (grey), $NF90_b$wt–NF45 (black) and $NF90_b^{S651E}$–NF45 (white), respectively. Newly synthesized [^{32}P]-labeled RNA products were extracted and analyzed by scintillation counting. The relative levels of induction of RNA synthesis are shown in comparison to the control reaction without complemented proteins. For each panel, the mean and standard deviations of three independent experiments are shown. (**) $P < 0.01$. Note, that a quantitative comparison of the signals obtained with poly(rC) and the other templates is not feasible as the experiments in (B, C) and (D) were performed with different types of radiolabeled nucleotides (see Materials and Methods section).

NF90 catalyzed RNA annealing is an enthalpy-driven process

We next sought to define the underlying mechanism of the NF90-catalyzed reaction. For this, we performed Arrhenius-analyses ('transition state-analyses'), which investigated the temperature-dependence of the RNA-annealing reactions in the absence and presence of protein. Apparent rate constants k_{obs} were normalized to the RNA or protein concentrations according to Doetsch *et al.* and the calculation of parameters was done by using Equations (4)-(7) (41). Thus, 'RNA only' reactions with the diverse HCV-SL3 and RaSc RNA variants (ds, fork and bulge) revealed that these shared the same properties in their individual transition states under the applied conditions. The activation energies E_A were between 4 and 7 kcal mol^{-1} and changes in entropy $\Delta S^{\#}$ ranged from –20 to –8 cal mol^{-1} K^{-1} (Supplementary Figure S4 and Table S3). Hence, we concluded that these data reflected a common situation for interactions of short, unstructured ssRNAs (41–43).

For the analyses of the protein-catalyzed reactions, we focused on the dsHCV-SL3 and RaSc substrates and tested the unmodified $NF90_b$ and $NF90_b$–NF45 as well as the modified $NF90_b^{S651E}$–NF45 complex. Interestingly, in the presence of each of the protein preparations, the activation energy E_A dropped to 0 kcal mol^{-1}. Moreover, and independently of the applied RNA substrates, the reactions were accompanied by a large decrease in the change of entropy, in which $NF90_b$wt showed the largest, $NF90_b$wt–NF45 showed the lowest, and $NF90_b^{S651E}$–NF45 showed an intermediate magnitude in $|\Delta\Delta S^{\#}|$ (Figure 3C and Table 4; for data with RaSc see Supplementary Figure S4C). In close congruence with the earlier shown annealing and strand displacement data, this yielded a stabilization of the transition state ($\Delta G^{\#}$) of 1 kcal mol^{-1} by $NF90_b$wt–NF45 and only 0.2 kcal mol^{-1} by $NF90_b^{S651E}$–NF45. In the presence of $NF90_b$wt, the transition state was actually destabilized by 0.6 kcal mol^{-1} as compared to the RNA-only situation (Table 4). Taken together, the data indicate that the RNA chaperone activity of $NF90_b$ depends on the presence of a functional C-terminus of the protein and on the formation of a heterodimer with NF45.

The RNA chaperone activity of $NF90_b$–NF45 supports hepatitis C virus RNA synthesis in vitro.

To gauge the biological relevance of the RCA of NF90, we addressed the protein's proposed role in the life cycle of HCV. As explained, NF90–NF45 was earlier shown to interact with the SL3 motif within the HCV genome's 3′UTR. SL3, together with SL2 and SL1 form the so-

Table 4. Arrhenius parameters of the RNA annealing reaction of dsHCV-SL3 and RaSc

	E_A (kcal mol^{-1})	$\Delta H^{\#}$ (kcal mol^{-1})	$\Delta S^{\#}$ (cal mol^{-1} K^{-1})	$\Delta G^{\#}{}_{20^\circ C}$* (kcal mol^{-1})
RNA only (dsHCV-SL3)	7.2 ± 1.6	6.6 ± 1.6	-8.6 ± 2.1	9.1
+ NF90	0 ± 0.1	− 0.6 ± 0.1	− 141.2 ± 23.6	9.7
+ NF90–NF45	0 ± 0.1	− 0.6 ± 0.1	− 117.1 ± 19.6	8.1
+ NF90^{S651E}–NF45	0 ± 0.1	− 0.6 ± 0.1	− 128.9 ± 21.5	8.9
RNA only (RaSc)	5.5 ± 0.9	4.9 ± 0.9	− 15.8 ± 2.9	9.5
+ NF90–NF45	0 ± 0.1	− 0.6 ± 0.1	− 108.5 ± 16.3	7.6

* The error in $\Delta G^{\#}$is less than 10%.

called 'X-tail' region of the HCV RNA at the immediate 3′-terminus, which is highly conserved among different HCV subtypes and essential for replication (44,45). The HCV 3′UTR additionally includes a variable polyU/UC stretch and a highly variable region at the 5′-end, which may form a labile stem-loop structure, termed here SL_{stop} ((6); Figure 4A). The 3′UTR was further shown to form complex, tertiary structures with RNA elements in the 3′-end of the viral protein-coding region. In particular, the stem-loop motif 5BSL3.2, which also interacts with the neighbored stem-loop 5BSL3.1 (46,47), forms a kissing-loop interaction with SL2 that is important for effective viral replication ((48,49); summarized by Sagan *et al.* (50); see Figures 4A and 5A).

NF90 was suggested to positively affect the first replication step of HCV, which, with all positive-strand RNA viruses involves the synthesis of a complementary negative-strand RNA intermediate by the viral RNA-dependent RNA polymerase (RdRp, (51)). Thus, to examine NF90 and NF90–NF45 for a direct effect on this step, we applied a well-established RdRp assay, which reconstitutes negative-strand RNA synthesis with the purified HCV RdRp NS5B and a viral RNA template *in vitro* (52–54). Recently, we used a similar approach to reveal the functional importance of an RCA activity of a cellular host factor involved in the replication of the HCV-related West Nile Flavivirus (28,55). The assay applied here was performed with an RNA template, which encodes the 3′UTR as well as the aforementioned 5BSL motifs of the HCV RNA (referred here to as '5BSL3_3UTR'; Figure 4A), i.e. the template contained all *cis*-acting replicative elements (CRE) known to be essential for the *de novo* initiation of HCV negative-strand RNA synthesis (50). As control-templates served a segment of the HCV RNA that encodes exclusively the 3′X-tail region ('X-tail'). As a positive control for the activity of NS5B, we applied poly(rC) RNA, which was known to represent a reasonable template of flaviviral polymerases (28,55).

Control 'template-only' RdRp assays confirmed that, with the 5BSL3_3UTR RNA and with the poly(rC) RNA nucleotide, incorporation/RNA synthesis was clearly detectable (Supplementary Figure S5). In contrast, the assays that were performed with the X-tail template or with the radiolabeled nucleotide alone yielded only background values indicating that a terminal transferase activity of the NS5B RdRp was undetectable under the chosen conditions (Supplementary Figure S5). Next, we pre-incubated the template RNAs with $NF90_b$wt, with $NF90_b$wt–NF45 or with the pseudophosphorylated $NF90_b^{S651E}$–NF45 and then started the RdRp reaction by adding the NS5B polymerase. Interestingly, with the 5BSL3_3UTR RNA and in the presence of $NF90_b$wt–NF45, the RdRp-catalyzed negative-strand-RNA synthesis was significantly stimulated, with a maximal increase of 2.5-fold. At lower concentrations of complex, the stimulatory effect correlated with the amounts of complemented $NF90_b$wt–NF45, while it was not detectable at very high concentrations of the heterodimer (Figure 4B). In contrast, neither $NF90_b$wt nor $NF90_b^{S651E}$–NF45 displayed a stimulatory effect on negative-strand-RNA synthesis with the 5BSL3_3UTR RNA. Moreover, in assays that were performed with the X-tail or the poly(rC) templates, none of the proteins caused changes in product yields, which excluded a direct effect of $NF90_b$wt–NF45 on the HCV NS5B RdRp (Figure 4C-D).

These data demonstrated an intrinsic specificity of $NF90_b$wt–NF45 as the complex stimulated the RdRp catalyzed synthesis of negative-strand RNA synthesis exclusively with the 5BSL3_3UTR template. Considering that $NF90_b$wt as well as $NF90_b^{S651E}$–NF45 each showed a lower RCA than $NF90_b$wt–NF45, the stimulatory effect on negative-strand-RNA synthesis correlated with the level of the protein's RNA chaperone activities.

$NF90_b$–NF45 changes the conformation of the HCV 5BSL3_3UTR RNA

The fact that the 3′-terminus of the HCV genome folds into complex secondary and tertiary RNA structures that involve the 3′UTR as well as the 3′-part of the NS5B coding region (Figure 4A) suggests that the initiation process of viral RNA synthesis by the RdRp is decisively determined by the RNA conformation (47,50,56). Along this line, we hypothesized that $NF90_b$wt–NF45 should be more capable than $NF90_b$wt and $NF90_b^{S651E}$–NF45 of changing the conformation of the viral RNA in such a way that this leads to an increase in replication-competent RNA conformers.

To address this, we decided to investigate the 5BSL3_3UTR RNA for global structural changes by analyzing its thermal melting behavior in the absence and presence of protein (57). Thus, the protein-free 5BSL3_3UTR RNA turned out to exhibit a flattened thermal denaturation profile (Figure 5A and B), and the transition midpoint was determined at 68°C from the first derivative of the transition curve (Figure 5C). Interestingly, in the presence of $NF90_b$wt–NF45, the thermal transition of the RNA exhibited at least two pronounced transition parts with midpoints at 58 and 68°C, respectively (Figure 5B and C). A third transition was indicated at $T > 80^\circ C$, but protein precipitation was observed at $T > 85^\circ C$, which hampered further interpretation. With $NF90_b$wt, similarly changed transition parts were detected, but, in comparison

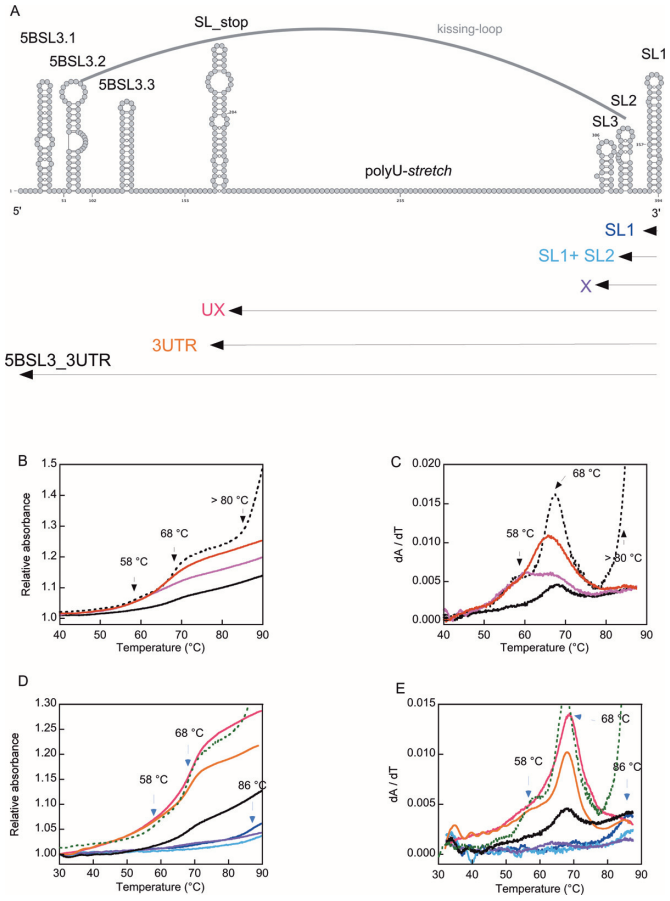

Figure 5. NF90$_b$wt–NF45 changes the conformation of the viral RNA template. (**A**) Schematic representation of the 3′-end of the HCV RNA genome as presented in Figure 4A. The panel below schematically shows the different segments of the 5BSL3_3UTR RNA that were used for thermal melting studies. (**B**) Thermal denaturation of 30 nM of 5BSL3_3UTR in the absence (black) and presence of 60 nM NF90$_b$wt (purple), NF90$_b$wt–NF45 (dashed line) or NF90$_b^{S651E}$–NF45 (red). The denaturation was recorded in the temperature range from 30 to 90°C in polymerase assay buffer at a wavelength of 268 nm. The relative absorbance to the value at 30°C is shown. (**C**) First derivative of the traces shown in (B) to determine the transition midpoints T_M (arrows). (**D**) Thermal denaturation of 30 nM of different segments of the 5BSL3_3UTR RNA (see panel A) was recorded in the temperature range from 30 to 90°C in polymerase assay buffer at 268 nm. The relative absorbance to the value at 30°C is shown. (**E**) First derivative of the traces shown in **(D)** to determine the transition midpoints T_M. In (D) and (E) the transition and first derivative of 5BSL3_3UTR in the presence of NF90$_b$wt–NF45 is also shown (dashed lines).

to NF90$_b$wt–NF45, the transition that occurred at T_M = 68°C was less pronounced, less cooperative, and the transition at T > 80°C was not detected (Figure 5B and C). With NF90$_b^{S651E}$–NF45, both transitions at T_M = 58 and 68°C were detectable, and the amplitude of the latter transition ranked in between that of NF90$_b$wt–NF45 and that of NF90$_b$wt. The transition at T > 80°C was also undetectable with NF90$_b^{S651E}$–NF45 (Figure 5B and C).

Since SHAPE (selective 2-hydroxyl acylation analyzed by primer extension, (58)) experiments failed to unambiguously detect NF90–NF45 mediated conformational transitions in the 5BSL3_3UTR RNA (Supplementary Figure S6), we assumed that the protein complex targets higher order rather than secondary RNA structures. To clarify this further, we analysed the thermal melting of individual segments of the RNA (Figure 5A) in the absence of protein. Thus, RNA transcripts that contained only SL1, SL1 + SL2 or the X-tail (X) did not display a cooperative transition while a segment, termed here as UX, which contained the X-tail and the polyU/UC region, revealed a pronounced profile with midpoints at 58 and 68°C, respectively (Figure 5D and E). A larger 3UTR segment, which additionally contained SL$_{stop}$ (see Figure 5A), displayed a similar cooperative thermal transition with a less prominent midpoint at 58°C and a pronounced midpoint at 68°C. Thus, it turned out that the melting behavior of the RNA segments UX and 3UTR resembled that of the 5BSL3_3UTR RNA in the presence of NF90wt–NF45 (see Figure 5D and E). Since 5BSL3_3UTR RNA only did not follow this melting profile, this suggested that NF90–NF45 mainly affected the fold of the 3′-portion of the viral RNA (see Discussion).

In conclusion, it can be stated that an evident change in thermal melting of the 5BSL3_3UTR RNA occurred in the presence of each of the purified proteins. The least alterations were monitored with the NF90$_b$ monomer, while intermediate changes occurred with NF90$_b^{S651E}$–NF45, and most pronounced changes were detected with NF90$_b$wt–NF45. As this order is congruent with the increasing efficiency of the protein's RCA, these findings strongly suggest a correlation between the protein's RCA and the observed structural changes in the viral RNA.

NF90$_b$–NF45 changes the conformation of the HSR-SL motif of VEGF-mRNA

As already outlined, NF90 was demonstrated to determine VEGF protein synthesis under hypoxia by binding to a regulatory element, designated as 'hypoxia stability region', HSR, within the mRNA's 3′UTR (Supplementary Figure S1A) (4). Interestingly, the HSR represents a riboswitch, i.e. its secondary structure may adopt at least two different conformations that display a lower or higher degree of base-pairing, the latter of which supports the translation of the mRNA (Figure 6A). NF90 was indicated to be an active part of this switch by stabilizing double-stranded conformations of the HSR (32). A key role in these transitions is played by a 63 nt element of the HSR, HSR-SL, which is capable of forming an extensive stem-loop structure (4; Figure 6A; Supplementary Figure S1A). Thus, for a further understanding of the relevance of NF90–NF45's RCA, the last set of experiments of this study aimed at determining its impact on the HSR-SL structure. For this, we followed the same approach as with the HCV-derived RNAs, namely by measuring transition curves in thermal melting experiments to define the thermodynamic parameters of HSR-SL in the absence and presence of NF90wt–NF45.

Since changes of the ionic strength affect base-paring and, accordingly, dsRNA formation (57,59,60), we measured first the thermal transitions of the HSR-SL at increasing ionic strengths in assay buffer only (Figure 6B). As expected, the melting temperature T_M increased with increasing concentrations of NaCl from 44°C at 0 mM to 58°C at 400 mM (Figure 6B). The corresponding ΔH_{TM} values,

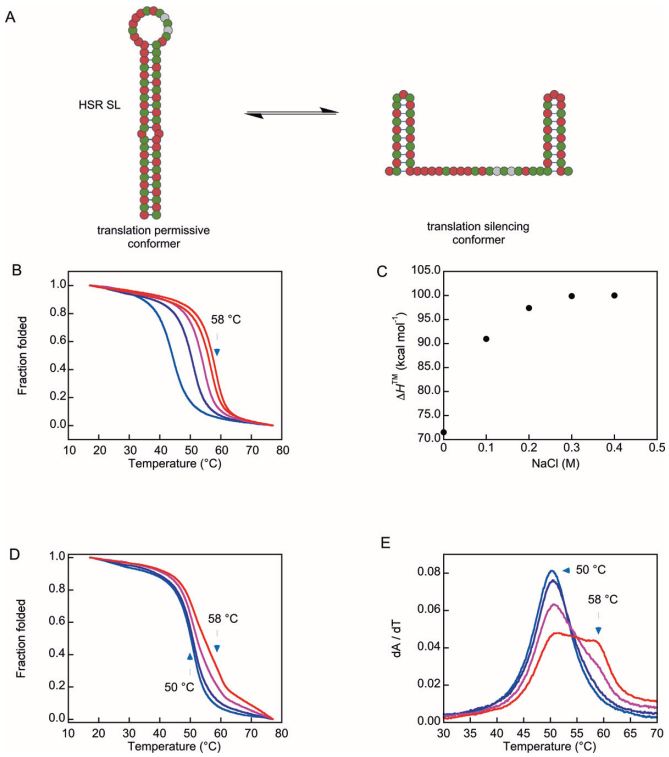

Figure 6. NF90wt–NF45 changes the conformation of the HSR element of the VEGF RNA. (**A**) Schematic representation of the applied HSR segment of the VEGF mRNA, which essentially comprised the main stem-loop structure HSR-SL. This element can adopt at least two different conformations, which show different availability for translation (63). Red, green and gray color indicate A, U and G/C nucleotides, respectively. (**B**) The thermal unfolding of 500 nM of the RNA was monitored at a wavelength of 268 nm in the temperature range from 10 to 90°C in assay buffer without (blue), or with 100 mM (purple), 200 mM (magenta), 300 mM (red) and 400 mM (orange) NaCl. The temperature gradient was 0.4 K min^{-1}. (**C**) Transition curves shown in (B) were investigated with Equations (8) and (9), which yielded the change in enthalpy ΔH_{TM} of melting the RNA. These were plotted versus the respective concentrations of NaCl. (**D**) The thermal melting of 500 nM HSR RNA in the absence (blue) and presence of 60 nM (purple), 120 nM (magenta) and 200 nM (red) $NF90_b$wt–NF45 were recorded in assay buffer supplemented with 100 mM NaCl applying the same conditions as in (B). (**E**) First derivative of the transition curves shown in (D). The arrows in (D) and (E) indicate apparent transition midpoints that were determined from the first derivative in (E).

which were obtained by applying Equations (8) and (9) (see Materials and Methods), interestingly followed a non-linear but hyperbolic dependency on the NaCl concentration that reached a maximum at above 200 mM (Figure 6C). ΔH_{TM} is proportional to the number of melting base pairs with a general approximation of $\Delta H = 4.6$–6.1 kcal mol^{-1} per bp (61,62). In the absence of NaCl, the ΔH_{TM} value of 71.5 kcal mol^{-1} accordingly corresponded to a melting of 11–15 bp, while at 400 mM NaCl, the ΔH_{TM} value of 100 kcal mol^{-1} corresponded to a melting of 16–21 bp (Figure 6C). Thus, in agreement with earlier findings of Ray *et al.* (63), these data indicated that at concentrations below 200 mM NaCl, the predominant conformation of the HSR-SL lacks the formation of 5 bp (Figure 6A). Interestingly, when we next measured the thermal transition of the HSR SL in the presence of increasing concentrations of NF90wt–NF45 at 100 mM NaCl, the T_M shifted from 50 to 58°C (Figure 6D and E). As this value corresponded exactly to that of the thermodynamically more stable conformation of the HSR-SL in the absence of protein, we took these data as an indication that NF90wt–NF45 actively populates and stabilizes a HSR conformation that contains a higher degree of base pairing (Figure 6A).

DISCUSSION

NF90 is an important post-transcriptional regulator of gene expression that exists predominantly in a complex with NF45. We showed earlier that the RNA-binding capacity of the heterodimer is considerably increased in comparison to the monomeric NF90. This was explained by conformational changes in NF90 upon binding of NF45 that increase the co-operative interplay between NF90's RBMs. Phosphorylation of Ser-651 within the C-terminal RGG/RG region was suggested to inhibit these conformational changes and demonstrated to be a clear-cut negative regulator of RNA-binding by NF90 and NF90–NF45 (15,19). During heterodimer formation, we furthermore observed a mutual stabilization of the proteins, which, however, could not explain the improved RNA-binding affinities (19).

Here, we obtained unequivocal evidence that NF90 has an inherent RNA chaperone activity, which functions particularly to anneal RNA. Interestingly, the RNA-annealing activity of NF90 also significantly improves by interaction with NF45, i.e. the efficiency of ssRNA hybridization by NF90–NF45 was found to be 50-fold increased in comparison to the monomeric NF90. On the one hand, we explained this by the improved RNA-binding affinity of the complex (19). On the other hand, we observed that complex formation stabilizes structural elements of NF90 that contribute to the RAA and acquired evidence that heterodimerization directly improves catalytic steps of the reaction (Figures 2 and 3, Table 4). In sum, these data provided solid evidence that the formation of the NF90–NF45 complex aids NF90's RCA.

Interestingly, both the NF90–NF45 heterodimer, as well as the monomeric NF90, display different RAA efficiencies on two different RNA pairs (Figure 1), which apparently arise from different on-rates (k_{on}) of substrate binding. This suggested a putative specificity in the reaction, and this idea was further strengthened when we performed the annealing assays with partly mismatching ssRNA substrates. These experiments demonstrated that structural features of the formed dsRNAs considerably affect the efficiency of the protein-catalyzed RNA-annealing reactions. NF90 and NF90–NF45 were further revealed to perform strand-displacement reactions only on mismatched dsRNAs to yield dsRNAs with a higher degree of base-pairing (Figure 3). NF90 and NF90–NF45 are accordingly suggested to function as substrate-selective RNA chaperones, which require a minimum region of consecutively formed base pairs in order to catalyze RNA annealing in the most efficient way.

The mechanisms of non-catalyzed RNA-annealing reactions of short, unstructured ssRNAs were earlier characterized to involve charge-repulsion ($\Delta H^{\#} > 0$) and a decrease in microstate dynamics ($\Delta S^{\#} < 0$), (41–43,64). We observed

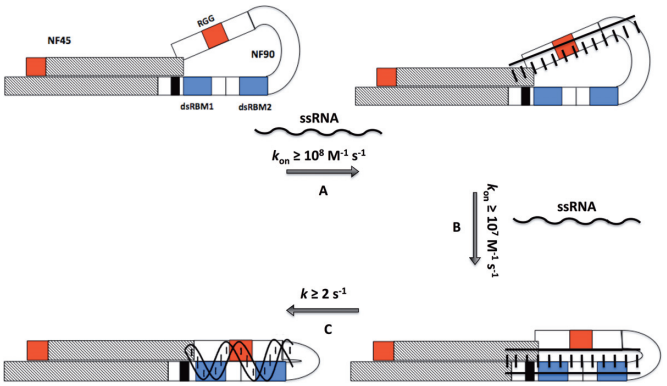

Figure 7. Model of the RNA chaperone activity of NF90$_b$wt–NF45. (**A**) Binding of the first ssRNA substrate is mediated by NF90's C-terminus, which results in the presentation of an annealing-competent conformation of the bound ssRNA. (19). (**B**) By binding the second ssRNA, the protein-RNA complex transitions into a closed conformation, which limits the reverse reaction and stabilizes the initial RNA-RNA contact ($\Delta S^{\#}_{NF90} << \Delta S^{\#}_{RNA}$). The restricted diffusion within the NF90$_b$wt–NF45-RNA complex and the annealing-competent conformation of the RNA facilitate initial base pair formation. (**C**) The heterodimer induces an accelerated transition into the final RNA duplex by applying a conformational pressure on the initially base paired RNAs to adopt a proper alpha-helical shape. This is suggested by the observation that an intra-molecular step is rate-limiting at high protein concentrations (Figure 1C). Indicated rate constants are based on data presented in Table 2 and by Schmidt et al. (19).

similar characteristic for RNA substrates used in this study. In contrast, in the presence of the different NF90 variants, a complete compensation of charge-repulsion was achieved ($\Delta H^{\#} \sim 0$ kcal mol^{-1}), and the dynamics of the system decreased even further ($\Delta S^{\#}_{NF90} << \Delta S^{\#}_{RNA}$). A similar situation was described for the RNA-annealing protein gBP21, which stabilizes ssRNA by compensating the negative charges of the RNA's backbone ($\Delta H^{\#} \sim 0$ kcal mol^{-1}) and induces local conformational changes within the ssRNA. The activity of gBP21 was interpreted as a 'matchmaker mechanism', i.e. the protein was proposed to render the ssRNA annealing-competent upon binding (64). Considering the earlier analyses of NF90's RNA binding properties (15), our data point to a highly rigid protein–RNA complex as the RNA-annealing reaction progresses and suggest that these complexes form a closed conformation-like state during the reaction (shown as a model in Figure 7). This would support a matchmaker mechanism by providing an annealing-competent microenvironment and result in an increase in k_{cat}. Interestingly, this was observed only for the catalysis by variants of NF90–NF45, supporting the conclusion that the NF90–NF45 interaction specifically fosters the formation of a closed conformation, as suggested earlier (19), and in this way directly facilitates the provision of an annealing-competent system (Figure 7). The importance of the C-terminal region of NF90 during these processes is highlighted by the observation that the pseudo-phosphorylated NF90$_b^{S651E}$–NF45 displays a lower tendency to form such a rigid protein-RNA complex and that it has a low RCA. In accord with this, NF90$_b\Delta$C63 does not show an RAA. Conversely, the dsRBM-impaired NF90$_b^{F432,559A}$–NF45 has a wild-type-like activity indicating that NF90's dsRBMs do not contribute to the actual catalysis of RNA annealing. However, considering the capability of dsRBMs to bind specifically A-helical RNA, it is conceivable that these motifs play a role after the rate-limiting step, for example, by stabilizing the dsRNA product (Figure 7).

The significance of the RCA of NF90 became apparent when we investigated the role of NF90 and NF90–NF45 during the initial step of the RNA replication process of HCV, the synthesis of viral negative-strand replicative intermediate, which can be reasonably reconstituted *in vitro*. The key enzyme catalyzing HCV RNA replication is the NS5B RdRp (52). Although the binding process of NS5B to HCV RNA and the template-dependent production of dsRNA product were studied already in detail (50,65–68), the molecular determinants that contribute to the *de novo* initiation of HCV RNA synthesis are not yet completely characterized. For example, the NS5B 'promoter region' for the initiation of negative-strand RNA synthesis has not yet been defined. Our thermal melting assays with the 5BSL3_3UTR RNA template revealed that NF90$_b$wt, the pseudo-phosphorylated NF90$_b^{S651E}$–NF45, as well as NF90$_b$wt–NF45, each significantly alter the RNA's conformation. As explained, the extent of these changes firmly correlated with the RCA of NF90. It was most pronounced with NF90$_b$wt–NF45, which, exclusively, stimulates NS5B-mediated RNA synthesis (Figure 4). Thus, it is tempting to conclude that a main function of the RCA of NF90–NF45 involves the population of a replication-permissive HCV RNA conformer. Along this line, NF90–NF45 may cooperate with other proteins such as EWSR1, which was proposed as having a similar function (69).

Currently, we can only speculate about how NF90$_b$wt–NF45-guided structural alterations in the viral RNA stimulate HCV RNA synthesis. While we cannot exactly define the RNA elements that are modulated by NF90–NF45, the thermal melting data suggest a scenario in which the X-tail region of the 5BSL3_3UTR RNA forms a conformation that is unraveled by NF90–NF45. Considering the fact that the SHAPE reactivity of the RNA remained unchanged in the presence of the proteins (Supplementary Figure S6), the activity of NF90–NF45 was suggested to affect the RNA's tertiary structure, while the secondary structure elements are maintained. This idea is supported by the observation that those RNA transcripts, which contained the X-tail and the poly U stretch (UX and 3UTR), exhibited a similar melting profile in the absence of protein as the 5BSL3_3UTR RNA in the presence of the NF90–NF45 complex (Figure 5). In the absence of protein, the melting profile of 5BSL3_3UTR was not indicative of major transitions. Earlier protein–RNA interaction studies indeed revealed NF90–NF45 to associate with SL3 within the X-tail region, but only in the presence of polyU/UC (6).

Strikingly, the stimulatory effect of NF90$_b$wt–NF45 on NS5B-mediated RNA synthesis was only detectable with RNA templates that contained all *cis*-replicative elements (CRE) within the 3′-end of the viral ORF and the 3′UTR, which were characterized to be essential for effective viral RNA replication (46–49). Besides excluding a direct effect of NF90–NF45 on NS5B, these data together with the melting analyses fuel the speculation that the heterodimer changes the earlier-mentioned pseudoknot interactions of

the stem-loop motif 5BSL3.2 with the X-tail region of the HCV RNA, which, in turn, may increase the efficiency of negative-strand RNA synthesis by the viral polymerase. This idea is supported by our data as well as by findings of other laboratories, which showed that the polymerase acts efficiently on RNA molecules that include the CRE, while the X-tail alone is a poor template (70–72). The complex tertiary structure formed by the CRE within the 3′-end of the viral ORF and the 3′UTR may be accordingly suggested as an important element of the NS5B promotor. The situation of the HCV 3′-end and the activity of NF90–NF45 could resemble what has been described with plant-infecting Tombusviruses. The genomic 3′-ends of these viruses encode a so-called 'replication silencer element' (RSE), a pseudoknot structure, which masks the promoter of the Tombusvirus RdRp (73). The Tombusvirus-encoded protein p33 was indicated to act as an RNA chaperone that rearranges the RSE to enable the polymerase to initiate negative-strand RNA synthesis efficiently (27).

Our findings further substantiate the idea that NF90 and NF90–NF45 have distinct functions in the cell. As NF45 significantly modulates the RNA-binding specificity (19), as well as the RNA-annealing activity of NF90 (this report), it may be reasonable to assume that most of the previously described functions of NF90 are exerted by the NF90–NF45 heterodimer. This notion fits to the earlier proposal of Guan et al. that NF45 has an important, hitherto disregarded, regulatory function by adjusting the cellular level and by steering the activity of the NF90–NF45 complex (17).

Combined with our earlier findings, the data presented here provide a general understanding of the activity of NF90–NF45. The modular architecture of NF90 facilitates a cooperative interplay of its RNA-binding domains, which enables specific RNA binding and a discrimination of structural RNA features (19). In turn, the mode of RNA-binding of NF90 determines its RCA by which the protein may change the conformation of the bound RNA. In this way, the heterodimer may affect inter- as well as intramolecular RNA-RNA interactions and accelerate cellular processes, which are otherwise trapped by non-functional or incorrect RNA structures. As several RNA targets of NF90–NF45 are likely to contain highly structured regions, association of the complex might also change the RNA's dynamics or even the distribution between different conformers of the bound RNA.

An interesting example, which was also addressed here, is the VEGF mRNA, where NF90–NF45 was suggested to bind to the HSR riboswitch element (4,63). Ray *et al.* obtained experimental evidence that, under hypoxia, this region transitions from a translation-silencing into a translation-permissive conformation (63), and studies of Yao *et al.* further indicated that NF90, being part of the HILDA protein complex, mediates the flipping of the riboswitch (32). In direct support of this, our data suggest that NF90wt–NF45 changes the structure of the HSR element *in vitro* such that, according to its substrate-selective RCA, the resulting conformer contains an increased number of base pairs. An increase of the double-stranded fraction of the HSR riboswitch was earlier shown to support the translation-permissive state of the VEGF mRNA (63).

A similar concept to what we propose here for NF90–NF45 was recently suggested to occur during early steps of ribosome assembly, where the ordered association of protein components to the maturing ribosome appears to be orchestrated by sequential protein-mediated conformations of the 16S ribosomal RNA (74). Protein-guided RNA dynamics were also shown to regulate processes in prokaryotes. The *E. coli* protein Hfq, one of the best-investigated proteins with RNA chaperone activity, was shown to be an efficient RNA '*annealer*' (75) and demonstrated to crucially affect the efficiency of translation initiation and stability of target mRNAs, both by hybridizing small regulatory RNAs to their target regions, as well as by stabilizing these complexes (76).

Very recently, NF90 was shown to promote the biogenesis of circular RNAs by binding to complementary intronic RNA pairs juxtaposing the exons that form the mature circular RNA (77). We suppose that the RCA of NF90–NF45 is critically involved in this process.

In conclusion, our data strongly support the opinion that the RCA of NF90 represents a major determinant of the protein's diverse biological activities. As shown here, the level of the RCA is regulated by post-translational processes such as phosphorylation, and by the association of NF45.

SUPPLEMENTARY DATA

Supplementary Data are available at NAR Online.

ACKNOWLEDGEMENTS

We thank Gary Sawers for critically reading of the manuscript and Christine Hamann for excellent technical assistance.

FUNDING

Deutsche Forschungsgemeinschaft [GRK 1026 to T.S., R.G.; BE1885/7, BE1885/12-1 to S.F., S.E.B.]; Martin Luther University Halle-Wittenberg (to R.G., S.F., S.E.B.). Funding for open access charge: Deutsche Forschungsgemeinschaft, Martin Luther University Halle-Wittenberg.
Conflict of interest statement. None declared.

REFERENCES

1. Kuwano,Y., Pullmann,R. Jr, Marasa,B.S., Abdelmohsen,K., Lee,E.K., Yang,X., Martindale,J.L., Zhan,M. and Gorospe,M. (2010) NF90 selectively represses the translation of target mRNAs bearing an AU-rich signature motif. *Nucleic Acids Res.*, **38**, 225–238.
2. Shi,L., Godfrey,W.R., Lin,J., Zhao,G. and Kao,P.N. (2007) NF90 regulates inducible IL-2 gene expression in T cells. *J. Exp. Med.*, **204**, 971–977.
3. Shi,L., Zhao,G., Qiu,D., Godfrey,W.R., Vogel,H., Rando,T.A., Hu,H. and Kao,P.N. (2005) NF90 regulates cell cycle exit and terminal myogenic differentiation by direct binding to the 3′-untranslated region of MyoD and p21WAF1/CIP1 mRNAs. *J. Biol. Chem.*, **280**, 18981–18989.
4. Vumbaca,F., Phoenix,K.N., Rodriguez-Pinto,D., Han,D.K. and Claffey,K.P. (2008) Double-stranded RNA-binding protein regulates vascular endothelial growth factor mRNA stability, translation, and breast cancer angiogenesis. *Mol. Cell. Biol.*, **28**, 772–783.
5. Gomila,R.C., Martin,G.W. and Gehrke,L. (2011) NF90 binds the dengue virus RNA 3′ terminus and is a positive regulator of dengue virus replication. *PLoS One*, **6**, e16687.

6. Isken,O., Baroth,M., Grassmann,C.W., Weinlich,S., Ostareck,D.H., Ostareck-Lederer,A. and Behrens,S.E. (2007) Nuclear factors are involved in hepatitis C virus RNA replication. *RNA*, **13**, 1675–1692.
7. Isken,O., Grassmann,C.W., Sarisky,R.T., Kann,M., Zhang,S., Grosse,F., Kao,P.N. and Behrens,S.E. (2003) Members of the NF90/NFAR protein group are involved in the life cycle of a positive-strand RNA virus. *EMBO J.*, **22**, 5655–5665.
8. Isken,O., Grassmann,C.W., Yu,H. and Behrens,S.E. (2004) Complex signals in the genomic 3′ nontranslated region of bovine viral diarrhea virus coordinate translation and replication of the viral RNA. *RNA*, **10**, 1637–1652.
9. Li,Y., Masaki,T., Shimakami,T. and Lemon,S.M. (2014) hnRNP L and NF90 interact with hepatitis C virus 5′-terminal untranslated RNA and promote efficient replication. *J. Virol.*, **88**, 7199–7209.
10. Masliah,G., Barraud,P. and Allain,F.H. (2013) RNA recognition by double-stranded RNA binding domains: a matter of shape and sequence. *Cell. Mol. Life Sci.: CMLS*, **70**, 1875–1895.
11. Ghisolfi,L., Joseph,G., Amalric,F. and Erard,M. (1992) The glycine-rich domain of nucleolin has an unusual supersecondary structure responsible for its RNA-helix-destabilizing properties. *J. Biol. Chem.*, **267**, 2955–2959.
12. Kiledjian,M. and Dreyfuss,G. (1992) Primary structure and binding activity of the hnRNP U protein: binding RNA through RGG box. *EMBO J.*, **11**, 2655–2664.
13. Reichman,T.W. and Mathews,M.B. (2003) RNA binding and intramolecular interactions modulate the regulation of gene expression by nuclear factor 110. *RNA*, **9**, 543–554.
14. Reichman,T.W., Muniz,L.C. and Mathews,M.B. (2002) The RNA binding protein nuclear factor 90 functions as both a positive and negative regulator of gene expression in mammalian cells. *Mol. Cell. Biol.*, **22**, 343–356.
15. Schmidt,T., Knick,P., Lilie,H., Friedrich,S., Golbik,R.P. and Behrens,S.E. (2016) Coordinated action of two double-stranded RNA binding motifs and an RGG motif enables nuclear factor 90 to flexibly target different RNA substrates. *Biochemistry*, **55**, 948–959.
16. Chaumet,A., Castella,S., Gasmi,L., Fradin,A., Clodic,G., Bolbach,G., Poulhe,R., Denoulet,P. and Larcher,J.C. (2013) Proteomic analysis of interleukin enhancer binding factor 3 (Ilf3) and nuclear factor 90 (NF90) interactome. *Biochimie*, **95**, 1146–1157.
17. Guan,D., Altan-Bonnet,N., Parrott,A.M., Arrigo,C.J., Li,Q., Khaleduzzaman,M., Li,H., Lee,C.G., Pe'ery,T. and Mathews,M.B. (2008) Nuclear factor 45 (NF45) is a regulatory subunit of complexes with NF90/110 involved in mitotic control. *Mol. Cell. Biol.*, **28**, 4629–4641.
18. Wolkowicz,U.M. and Cook,A.G. (2012) NF45 dimerizes with NF90, Zfr and SPNR via a conserved domain that has a nucleotidyltransferase fold. *Nucleic Acids Res.*, **40**, 9356–9368.
19. Schmidt,T., Knick,P., Lilie,H., Friedrich,S., Golbik,R.P. and Behrens,S.E. (2017) The properties of the RNA-binding protein NF90 are considerably modulated by complex formation with NF45. *Biochem. J.*, **474**, 259–280.
20. Rajkowitsch,L., Chen,D., Stampfl,S., Semrad,K., Waldsich,C., Mayer,O., Jantsch,M.F., Konrat,R., Blasi,U. and Schroeder,R. (2007) RNA chaperones, RNA annealers and RNA helicases. *RNA Biol.*, **4**, 118–130.
21. Rajkowitsch,L. and Schroeder,R. (2007) Dissecting RNA chaperone activity. *RNA*, **13**, 2053–2060.
22. Russell,R. (2008) RNA misfolding and the action of chaperones. *Front. Biosci.*, **13**, 1–20.
23. Cruceanu,M., Urbaneja,M.A., Hixson,C.V., Johnson,D.G., Datta,S.A., Fivash,M.J., Stephen,A.G., Fisher,R.J., Gorelick,R.J., Casas-Finet,J.R. *et al.* (2006) Nucleic acid binding and chaperone properties of HIV-1 Gag and nucleocapsid proteins. *Nucleic Acids Res.*, **34**, 593–605.
24. Daros,J.A. and Flores,R. (2002) A chloroplast protein binds a viroid RNA in vivo and facilitates its hammerhead-mediated self-cleavage. *EMBO J.*, **21**, 749–759.
25. Karakasiliotis,I., Chaudhry,Y., Roberts,L.O. and Goodfellow,I.G. (2006) Feline calicivirus replication: requirement for polypyrimidine tract-binding protein is temperature-dependent. *J. Gen. Virol.*, **87**, 3339–3347.
26. Zuniga,S., Sola,I., Cruz,J.L. and Enjuanes,L. (2009) Role of RNA chaperones in virus replication. *Virus Res.*, **139**, 253–266.
27. Stork,J., Kovalev,N., Sasvari,Z. and Nagy,P.D. (2011) RNA chaperone activity of the tombusviral p33 replication protein facilitates initiation of RNA synthesis by the viral RdRp in vitro. *Virology*, **409**, 338–347.
28. Friedrich,S., Schmidt,T., Geissler,R., Lilie,H., Chabierski,S., Ulbert,S., Liebert,U.G., Golbik,R.P. and Behrens,S.E. (2014) AUF1 p45 promotes West Nile virus replication by an RNA chaperone activity that supports cyclization of the viral genome. *J. Virol.*, **88**, 11586–11599.
29. Vogt,A.D. and Di Cera,E. (2012) Conformational selection or induced fit? A critical appraisal of the kinetic mechanism. *Biochemistry*, **51**, 5894–5902.
30. Grassmann,C.W., Yu,H., Isken,O. and Behrens,S.E. (2005) Hepatitis C virus and the related bovine viral diarrhea virus considerably differ in the functional organization of the 5′ non-translated region: implications for the viral life cycle. *Virology*, **333**, 349–366.
31. Riechmann,L., Lavenir,I., de Bono,S. and Winter,G. (2005) Folding and stability of a primitive protein. *J. Mol. Biol.*, **348**, 1261–1272.
32. Yao,P., Potdar,A.A., Ray,P.S., Eswarappa,S.M., Flagg,A.C., Willard,B. and Fox,P.L. (2013) The HILDA complex coordinates a conditional switch in the 3′-untranslated region of the VEGFA mRNA. *PLoS Biol.*, **11**, e1001635.
33. Shamanna,R.A., Hoque,M., Lewis-Antes,A., Azzam,E.I., Lagunoff,D., Pe'ery,T. and Mathews,M.B. (2011) The NF90/NF45 complex participates in DNA break repair via nonhomologous end joining. *Mol. Cell. Biol.*, **31**, 4832–4843.
34. Eguchi,Y. and Tomizawa,J. (1990) Complex formed by complementary RNA stem-loops and its stabilization by a protein: function of CoIE1 Rom protein. *Cell*, **60**, 199–209.
35. Eguchi,Y., Itoh,T. and Tomizawa,J. (1991) Antisense RNA. *Annu. Rev. Biochem.*, **60**, 631–652.
36. Attri,P., Venkatesu,P. and Lee,M.J. (2010) Influence of osmolytes and denaturants on the structure and enzyme activity of alpha-chymotrypsin. *J. Phys. Chem. B*, **114**, 1471–1478.
37. Golbik,R., Fischer,G. and Fersht,A.R. (1999) Folding of barstar C40A/C82A/P27A and catalysis of the peptidyl-prolyl cis/trans isomerization by human cytosolic cyclophilin (Cyp18). *Protein Sci.*, **8**, 1505–1514.
38. Bycroft,M., Grunert,S., Murzin,A.G., Proctor,M. and St Johnston,D. (1995) NMR solution structure of a dsRNA binding domain from Drosophila staufen protein reveals homology to the N-terminal domain of ribosomal protein S5. *EMBO J.*, **14**, 3563–3571.
39. Krovat,B.C. and Jantsch,M.F. (1996) Comparative mutational analysis of the double-stranded RNA binding domains of Xenopus laevis RNA-binding protein A. *J. Biol. Chem.*, **271**, 28112–28119.
40. Ramos,A., Grunert,S., Adams,J., Micklem,D.R., Proctor,M.R., Freund,S., Bycroft,M., St Johnston,D. and Varani,G. (2000) RNA recognition by a Staufen double-stranded RNA-binding domain. *EMBO J.*, **19**, 997–1009.
41. Doetsch,M., Furtig,B., Gstrein,T., Stampfl,S. and Schroeder,R. (2011) The RNA annealing mechanism of the HIV-1 Tat peptide: conversion of the RNA into an annealing-competent conformation. *Nucleic Acids Res.*, **39**, 4405–4418.
42. Eckardt,S., Romby,P. and Sczakiel,G. (1997) Implications of RNA structure on the annealing of a potent antisense RNA directed against the human immunodeficiency virus type 1. *Biochemistry*, **36**, 12711–12721.
43. Patzel,V. and Sczakiel,G. (1999) Length dependence of RNA-RNA annealing. *J. Mol. Biol.*, **294**, 1127–1134.
44. Kolykhalov,A.A., Mihalik,K., Feinstone,S.M. and Rice,C.M. (2000) Hepatitis C virus-encoded enzymatic activities and conserved RNA elements in the 3′ nontranslated region are essential for virus replication in vivo. *J. Virol.*, **74**, 2046–2051.
45. Blight,K.J. and Rice,C.M. (1997) Secondary structure determination of the conserved 98-base sequence at the 3′ terminus of hepatitis C virus genome RNA. *J. Virol.*, **71**, 7345–7352.
46. Diviney,S., Tuplin,A., Struthers,M., Armstrong,V., Elliott,R.M., Simmonds,P. and Evans,D.J. (2008) A hepatitis C virus cis-acting replication element forms a long-range RNA-RNA interaction with upstream RNA sequences in NS5B. *J. Virol.*, **82**, 9008–9022.
47. Tuplin,A., Struthers,M., Simmonds,P. and Evans,D.J. (2012) A twist in the tail: SHAPE mapping of long-range interactions and structural rearrangements of RNA elements involved in HCV replication. *Nucleic Acids Res.*, **40**, 6908–6921.

48. Friebe,P., Boudet,J., Simorre,J.P. and Bartenschlager,R. (2005) Kissing-loop interaction in the 3′ end of the hepatitis C virus genome essential for RNA replication. *J. Virol.*, **79**, 380–392.
49. You,S., Stump,D.D., Branch,A.D. and Rice,C.M. (2004) A cis-acting replication element in the sequence encoding the NS5B RNA-dependent RNA polymerase is required for hepatitis C virus RNA replication. *J. Virol.*, **78**, 1352–1366.
50. Sagan,S.M., Chahal,J. and Sarnow,P. (2015) cis-Acting RNA elements in the hepatitis C virus RNA genome. *Virus Res.*.
51. Lindenbach,B.D., Thiel,H.J. and und Rice,C.M. (2007) In: Howley,DMKAPM (ed). *Fields Virology*. 5th edn. Lippincott-Raven Publishers, Philadelphia.
52. Behrens,S.E., Tomei,L. and De Francesco,R. (1996) Identification and properties of the RNA-dependent RNA polymerase of hepatitis C virus. *EMBO J.*, **15**, 12–22.
53. Lohmann,V., Korner,F., Herian,U. and Bartenschlager,R. (1997) Biochemical properties of hepatitis C virus NS5B RNA-dependent RNA polymerase and identification of amino acid sequence motifs essential for enzymatic activity. *J. Virol.*, **71**, 8416–8428.
54. Oh,J.W., Ito,T. and Lai,M.M. (1999) A recombinant hepatitis C virus RNA-dependent RNA polymerase capable of copying the full-length viral RNA. *J. Virol.*, **73**, 7694–7702.
55. Friedrich,S., Schmidt,T., Schierhorn,A., Lilie,H., Szczepankiewicz,G., Bergs,S., Liebert,U.G., Golbik,R.P. and Behrens,S.E. (2016) Arginine methylation enhances the RNA chaperone activity of the West Nile virus host factor AUF1 p45. *RNA*, **22**, 1574–1591.
56. Tuplin,A., Struthers,M., Cook,J., Bentley,K. and Evans,D.J. (2015) Inhibition of HCV translation by disrupting the structure and interactions of the viral CRE and 3′ X-tail. *Nucleic Acids Res.*, **43**, 2914–2926.
57. Mergny,J.L. and Lacroix,L. (2003) Analysis of thermal melting curves. *Oligonucleotides*, **13**, 515–537.
58. Wilkinson,K.A., Merino,E.J. and Weeks,K.M. (2006) Selective 2′-hydroxyl acylation analyzed by primer extension (SHAPE): quantitative RNA structure analysis at single nucleotide resolution. *Nat. Protoc.*, **1**, 1610–1616.
59. Draper,D.E., Grilley,D. and Soto,A.M. (2005) Ions and RNA folding. *Annu. Rev. Biophys. Biomol. Struct.*, **34**, 221–243.
60. Tinoco,I. Jr and Bustamante,C. (1999) How RNA folds. *J. Mol. Biol.*, **293**, 271–281.
61. Hargittai,M.R., Gorelick,R.J., Rouzina,I. and Musier-Forsyth,K. (2004) Mechanistic insights into the kinetics of HIV-1 nucleocapsid protein-facilitated tRNA annealing to the primer binding site. *J. Mol. Biol.*, **337**, 951–968.
62. Rouzina,I. and Bloomfield,V.A. (1999) Heat capacity effects on the melting of DNA. 1. General aspects. *Biophys. J.*, **77**, 3242–3251.
63. Ray,P.S., Jia,J., Yao,P., Majumder,M., Hatzoglou,M. and Fox,P.L. (2009) A stress-responsive RNA switch regulates VEGFA expression. *Nature*, **457**, 915–919.
64. Muller,U.F. and Goringer,H.U. (2002) Mechanism of the gBP21-mediated RNA/RNA annealing reaction: matchmaking and charge reduction. *Nucleic Acids Res.*, **30**, 447–455.
65. Mosley,R.T., Edwards,T.E., Murakami,E., Lam,A.M., Grice,R.L., Du,J., Sofia,M.J., Furman,P.A. and Otto,M.J. (2012) Structure of hepatitis C virus polymerase in complex with primer-template RNA. *J. Virol.*, **86**, 6503–6511.
66. Paul,D., Madan,V. and Bartenschlager,R. (2014) Hepatitis C virus RNA replication and assembly: living on the fat of the land. *Cell Host Microbe*, **16**, 569–579.
67. Reich,S., Golbik,R.P., Geissler,R., Lilie,H. and Behrens,S.E. (2010) Mechanisms of activity and inhibition of the hepatitis C virus RNA-dependent RNA polymerase. *J. Biol. Chem.*, **285**, 13685–13693.
68. Reich,S., Kovermann,M., Lilie,H., Knick,P., Geissler,R., Golbik,R.P., Balbach,J. and Behrens,S.E. (2014) Initiation of RNA synthesis by the hepatitis C virus RNA-dependent RNA polymerase is affected by the structure of the RNA template. *Biochemistry*, **53**, 7002–7012.
69. Oakland,T.E., Haselton,K.J. and Randall,G. (2013) EWSR1 binds the hepatitis C virus cis-acting replication element and is required for efficient viral replication. *J. Virol.*, **87**, 6625–6634.
70. Zhong,W., Uss,A.S., Ferrari,E., Lau,J.Y. and Hong,Z. (2000) De novo initiation of RNA synthesis by hepatitis C virus nonstructural protein 5B polymerase. *J. Virol.*, **74**, 2017–2022.
71. Kim,M., Kim,H., Cho,S.P. and Min,M.K. (2002) Template requirements for de novo RNA synthesis by hepatitis C virus nonstructural protein 5B polymerase on the viral X RNA. *J. Virol.*, **76**, 6944–6956.
72. Oh,J.W., Sheu,G.T. and Lai,M.M. (2000) Template requirement and initiation site selection by hepatitis C virus polymerase on a minimal viral RNA template. *J. Biolog. Chem.*, **275**, 17710–17717.
73. Pogany,J., Fabian,M.R., White,K.A. and Nagy,P.D. (2003) A replication silencer element in a plus-strand RNA virus. *EMBO J.*, **22**, 5602–5611.
74. Kim,H., Abeysirigunawarden,S.C., Chen,K., Mayerle,M., Ragunathan,K., Luthey-Schulten,Z., Ha,T. and Woodson,S.A. (2014) Protein-guided RNA dynamics during early ribosome assembly. *Nature*, **506**, 334–338.
75. Updegrove,T.B., Zhang,A. and Storz,G. (2016) Hfq: the flexible RNA matchmaker. *Curr. Opin. Microbiol.*, **30**, 133–138.
76. Vogel,J. and Luisi,B.F. (2011) Hfq and its constellation of RNA. *Nat. Rev. Microbiol.*, **9**, 578–589.
77. Li,X., Liu,C.X., Xue,W., Zhang,Y., Jiang,S., Yin,Q.F., Wei,J., Yao,R.W., Yang,L. and Chen,L.L. (2017) Coordinated circRNA biogenesis and function with NF90/NF110 in viral infection. *Mol. Cell*, **67**, 214–227.